

IFUM-871/FT
 FTUAM-02-459
 ULB-02-167

Analysis of Neutrino Oscillation Data with the Recent KamLAND results

P. Aliani^{†1}, V. Antonelli^{★1}, R. Ferrari^{★1}, M. Picariello^{★1}, E. Torrente-Lujan^{◎1}

[†] *Service de Physique Théorique, Univ. Libre de Bruxelles, Bruxelles, Belgium,*

[★] *Dip. di Fisica, Univ. di Milano, and INFN Sez. Milano, Via Celoria 16, Milano, Italy*

[◎] *Dept. de Fisica, Grupo de Fisica Teorica, Univ. de Murcia, Murcia, Spain*

Abstract

We present an updated analysis of all available solar and reactor neutrino data, emphasizing in particular the totality of the KamLAND results and including the *SNO* phase III spectrum data. In a two active-neutrino framework, we determine the solutions in the Δm_{\odot}^2 , $\tan^2 \theta_{\odot}$ parameter space compatible with experimental data using a ϕ -distribution technique where the gaussian approximation is not acceptable. Combining all data, we obtain the following best-fit parameters: $\Delta m_{\odot}^2 = 8.17 * 10^{-5}$, $\tan^2 \theta_{\odot} = 0.40$

PACS: 26.65.+t, 14.60.Pq

1 Introduction

New evidence of antineutrino disappearance in a beam of antineutrinos in the Kamland experiment has been presented [1]. The analysis of the experimental results on reactor physics and solar neutrinos [2] in terms of neutrino oscillations has largely improved our knowledge of neutrino mixing. Moreover the recent KamLAND results confirm the previous results and give a more stringent limit on the neutrino mass parameters.

The solar neutrino data prior to September 7, 2003 converged to two distinct regions in the parameter space, often referred to as LMAI (centered around the best-fit point of $\Delta m_{\odot}^2 = 7.1 \times 10^{-5}$ eV², $\tan^2 \theta_{\odot} = 0.47$) and LMAII (centered around $\Delta m_{\odot}^2 = 1.5 \times 10^{-4}$ eV², $\tan^2 \theta_{\odot} = 0.48$). The inclusion of the last year's SNO data effectively eliminated the LMAII region at 4σ . The ambiguity present in the Δm_{\odot}^2 parameter which was a result of incorporating the KamLAND data to the Solar neutrino data had disappeared. The recent kamLAND results modify the best-fit point position in the parameter space and give a $\Delta m_{\odot}^2 = 8.0 \times 10^{-5}$ eV², $\tan^2 \theta_{\odot} = 0.40$. The aim of this work is to present a comprehensive updated analysis of all recent solar neutrino data including the KamLAND reactor-experiment results to determine the extent of the remaining viable region in the parameter space.

The structure of this work is the following: in section 2 we briefly review our approach to the analysis of the KamLAND data.

In section 3 we discuss the importance of the SNO data and the spectrum results, and all other solar and non-solar experiments taken into consideration. We then proceed, in section 4, to explain the procedure adopted in our analysis and in section 5 we present our results. Finally we summarize and conclude in section 6.

¹e-mails: paola.aliani@ulb.ac.be, vito.antonelli@mi.infn.it, marco.picariello@mi.infn.it, emilio.torrente-lujan@cern.ch

1.1 The Sudbury Neutrino Observatory

The Sudbury Neutrino Observatory (SNO) collaboration has presented data relative to the NaCl phase of the experiment [3]. The addition of NaCl to a pure D₂O detection medium has the effect of increasing the detector's sensitivity to the neutral-current (NC) reactions within its fiducial volume. The NC detection efficiency has changed from a previous 'no-salt' phase of approximately a factor three (the efficiency being a position-related quantity, we see that the increase is even bigger for distant events (see fig. 1a of [3]). This novelty has made it possible for the SNO collaboration to analyze their data without making use of the no-spectrum-distortion hypothesis. Furthermore, they have adopted a new 'event topology' criterion to distinguish among the different channels within the detector.

The SNO detector was planned to run on a three-phase program (for a comprehensive coverage of the SNO potentiality, see [4]). Being a heavy-water Cherenkov detector, it is sensitive to three neutrino interactions: elastic scattering (ES) $\nu_w + e^- \rightarrow \nu_x + e^-$, charged-current (CC) $\nu_e + d \rightarrow e^- + 2p$ and neutral current (NC) $\nu_x + d \rightarrow p + n + \nu_x$. During the first phase of operation, data relative only to the first two of these was collected [5]. Successively, the NC reaction was tagged [6]. This reaction, which is equally sensitive to all neutrino flavors, is a fundamental experimental result, as it not only gives a direct measurement of the ⁸B flux, but also represents a direct measurement of non-electron-flavor neutrinos originating in the sun. Unfortunately, although the second-phase results proved essential in confirming the oscillation hypothesis, the efficiency with which the NC reactions were detected at SNO was quite low. The results depended heavily on the explicit assumption that the neutrino spectrum be non-distorted, an assumption that is fortunately true in the LMA region of the parameter space although misleading in the MSW regime. It was perhaps this observation that pushed certain authors to analyze the effects of varying the weight of the matter interaction term in the neutrino propagation Hamiltonian [7]. In this context, it was shown that despite the extraordinary amount of solar neutrino data in our possession, if a fit to different 'weights' of the matter interaction term did not prefer in a significant way the classical MSW solution, and in fact, the data did not exclude the no-MSW effect hypothesis [7]. This analysis has been carried out again with the new SNO data. The inclusion of this data seems to exclude the null hypothesis at 5.6σ [8].

The addition of NaCl to the pure heavy water in the SNO detector has the effect of drastically increasing the detector's sensitivity to the NC reaction. The ³⁵Cl acting as receptors for the neutrons emitted in the NC reaction, produce a cascade of photons which are easier to detect. The NC signal was tagged as being a 'multiple- γ ' event as opposed to the 'single- γ ' CC and ES signals in this new data set.

The SNO Collaboration has now devised a new data-analysis technique which relies on the topology of the three different events. The new parameter (β_ℓ) relative to which they marginalize is known as the 'isotropy' of the Cherenkov light distribution was used to separate the CC, ES and NC signals, something that was not possible in the previous two data sets. The measured fluxes as reported in [3] are:

$$\begin{aligned}\phi_{\text{CC}}^{\text{SNO}} &= 1.59_{-0.07}^{+0.08} \text{ (stat)} {}^{+0.06}_{-0.08} \text{ (syst)} \\ \phi_{\text{ES}}^{\text{SNO}} &= 2.21_{-0.26}^{+0.31} \text{ (stat)} \pm 0.10 \text{ (syst)} \\ \phi_{\text{NC}}^{\text{SNO}} &= 5.21 \pm 0.27 \text{ (stat)} \pm 0.38 \text{ (syst)}\end{aligned}\quad (1)$$

(2)

yielding a CC/NC ratio of

$$\phi_{\text{CC}}^{\text{SNO}} / \phi_{\text{NC}}^{\text{SNO}} = 0.306 \pm 0.026 \text{ (stat)} \pm 0.38 \text{ (syst)} \quad (3)$$

For the purpose of their analyzes, the SNO collaboration did not make use of the spectral information to produce their contour plots (see the SNO HOWTO for details [9]), both for simplicity and scarcity of information contained in the data itself. Nonetheless, we make use of all published data and refer the reader to section 4 for details.

The comparison of the new SNO results and the previous phase-II data can easily be made because the SNO collaboration has included in the recent paper results which were obtained following their previous method, along with the new unconstrained data. The new results are compatible with the previous ones. It seems that the overall effect of un-constraining the analysis is an increase in the measured fluxes, although the estimated total Φ_B has decreased relative to the previous best-fit value, leaving even less space for eventual sterile neutrinos.

2 KamLAND

2.1 The experimental setup

Reactor anti-neutrinos with energies above 1.8 MeV produced in some 53 commercial reactors are detected in the KamLAND detector via the inverse β -decay reaction $\bar{\nu}_e + p \rightarrow n + e^+$. The mean reactor-detector distance and energy window of these $\bar{\nu}_e$ makes KamLAND an ideal testing ground for the LMA region of the ν_\odot parameter space. The first results published by the KamLAND collaboration eliminated all possible solutions to the solar neutrino problem (SNP) except the LMA region of the parameter space [10]. The sensitivity of this experiment to the Δm^2 parameter divided the previously whole LMA region into two distinct regions, the one relative to the smaller mass-squared difference being preferred by data [11].

Recently, the KamLAND collaboration has announced the new results: they give the results of the data taken from October to Jan 2004, corresponding to about 317 days live time. The collaboration has taken all data and in the analysis, has included the previous set. The most significant changes in the analysis technique are related to the fiducial volume definition. Whereas in the previous work, events taking place at the outer edge of the nylon balloon were rejected, the recent analysis adopts a more sophisticated coincidence-measurement technique to exclude unwanted backgrounds. The estimated error on initial $\phi_0(\bar{\nu}_e)$ is of 2%, and a discussion between scientists and representatives of the commercial reactors has allowed the KamLAND collaboration to estimate the incoming neutrino flux with better accuracy. A graph of the variation of initial flux throughout the period of data taking is shown in fig. 1.a of [1].

2.1.1 Our simulations

In order to correctly model the detector and incorporate it into our solar neutrino analysis, we used a constant, time-averaged fuel composition for all of the commercial reactors within detectable distance of the Kamioka site, namely $^{235}\text{U} = 56.3\%$, $^{238}\text{U} = 7.9\%$, $^{239}\text{Pu} = 30.1\%$, and $^{241}\text{Pu} = 5.7\%$. We used the full cross-section including electron recoil corrections. We analyzed the data above threshold of 2.6 MeV than expected, as the low-energy end of the spectrum had effectively no events. We exclude the last bin. We neglected all backgrounds in our analysis, including geological background above 2.6 MeV. We use the resolutions published by the collaboration for the two different data sets, namely $\sigma(E) = 6.2\%/\sqrt{E}$ for the recent data and $\sigma(E) = 7.3\%/\sqrt{E}$ for data previously published.

In order to use all the data available, we use our montecarlo to estimate an equivalent efficiency for the two pre-upgrade and post-upgrade phases. In this way, we can determine an effective efficiency which takes the upgrade into account. The information relative to the no-oscillation initial flux for the two periods can be extracted from fig. 1.a of [1]. In their report, the collaboration gives an energy resolution σ/E of about 6.2% at 1 MeV, and bins ranging from 1.8 MeV to 8.5 MeV, although the lower energy bins are more affected by geo-neutrino backgrounds and are excluded from the analysis. The total systematic error is estimated at 6.5%. The spectrum can be deduced from fig. 2.a of [1] and is summarized in table 4. The collaboration adopts a hybrid statistical technique to account for the non-gaussian high energy bins, where the number of events are insufficient. The measure suited to samples from a multinomial distribution, the Pearson chi-square, can be generalized to work with samples from arbitrary asymptotic

multivariate distributions. This corresponds to the transition from independent system to correlated one. Because we want to take into account the correlation between the systematic errors, we do not use the Pearson chi-square, but his generalization. We consider the generalized ϕ -distribution in order to take systematic effects into account, and assume full correlation between the different bins.

No MSW effects are taken into consideration for the kamLAND data alone, as it was shown that any asymmetry due to matter effects is negligible for Δm^2 of the order of 10×10^{-5} eV².

3 Solar data

The most ponderous data present in our analysis comes from the solar neutrino experiments. The experimental results are compared to an expected signal which we compute numerically by convoluting the solar neutrino fluxes [17], oscillation probability at the detector location and detector response functions. Details of the numerical techniques used in this analysis can be found elsewhere [18]. Double-binned day-night and zenith angle bins are computed in order to analyze the full SuperKamiokande data [19], whereas single-binned data is used for the SNO detector [3]. The global signals only are used for the radiochemical experiments Homestake [12], SAGE [13, 14], GallEX [15] and GNO [16]. In particular, we want to draw attention to the fact that we have used both the global *and* the spectrum data of the recent SNO results, in order to make comparison with our previous analyzes more transparent.

4 Our analysis

We use a standard χ^2 technique to test the non-oscillation hypothesis. Two different sets of analyses are possible with the present data on neutrino oscillations: 1) solar data including the SK spectrum and previous phase-II SNO spectrum but not the SNO spectrum, combined with new the kamLAND spectrum 2) solar data including the SK spectrum and previous phase-II SNO spectrum and the SNO spectrum. We consider the phase-II and phase-III data as two distinct but fully correlated experiments.

In all cases, the χ^2 for the global rates of the radiochemical experiments are

$$\chi_{\text{rad}}^2 = (\mathbf{R}^{\text{th}} - \mathbf{R}^{\text{exp}})^T (\sigma_{\text{corr}} + \sigma_{\text{uncor}})^{-1} (\mathbf{R}^{\text{th}} - \mathbf{R}^{\text{exp}}), \quad (4)$$

where $\mathbf{R}^{\text{th,exp}}$ are length-two vectors containing the theoretical (or experimental) signal-to-no-oscillation expectation for the chlorine and gallium experiments. Correlated systematic and uncorrelated statistical errors are considered in σ_{syst} and σ_{stat} respectively. Note that the parameter-dependent R^{th} is an averaged day-night quantity, as the radiochemical experiments are not sensitive to day-night variations.

We consider the double-binned SK spectrum comprising of 8 energy bins for a total of 6 night bins and one day bin. The χ^2 is given by

$$\chi_{\text{SK}}^2 = (\alpha \mathbf{R}^{\text{th}} - \mathbf{R}^{\text{exp}})^T (\sigma_{\text{unc}}^2 + \sigma_{\text{cor}}^2)^{-1} (\alpha \mathbf{R}^{\text{th}} - \mathbf{R}^{\text{exp}}). \quad (5)$$

The covariance matrix σ is a 4-rank tensor containing information relative to the statistical errors and energy and zenith-angle bin-correlated and uncorrelated uncertainties. Since the publication of the first SNO NC results, we have adopted their estimate of ϕ_B and incorporated the new parameter α in the χ^2 representing the normalization with respect to this quantity. In determining our best-fit points, we minimize with respect to it.

As discussed in section 2.1.1, we use an alternative technique for the KamLAND data due to the low statistics of the high energy bins. Furthermore, in order to use all the available data, we determine overall detector efficiencies for the pre- and post- PMT/electronics upgrade phases and use them subsequently in our analysis.

The total KamLAND contribution to the χ^2 is therefore:

$$\chi_{\text{KL}}^2 = \chi_{\text{KL,glob}}^2 + \chi_{\text{KL},\phi}^2 \quad (6)$$

where

$$\chi_{\text{KL,glob}}^2 = \frac{(R^{\text{th}} - R^{\text{exp}})^2}{\sigma_{\text{stat+sys}}^2} \quad (7)$$

In the evaluation of $\chi_{\text{KL},\phi}^2$ we use vectors that comprise therefor of 13 spectral points of width 0.425 MeV. We have studied the influence of the systematic errors on the KamLAND response function and incorporated them in our correlation matrix. We assume full correlation among the different bins. Note that we use quantities that contain the number of events normalized to the no-oscillation scenario. Due to the fact that at high energy KamLAND observe a small number of events, we cannot use a Gaussian approximation for all bins. This means that the correlated systematic deviations cannot be introduced in a straightforward way. The ϕ -distribution is introduced for those bins and refer the reader to [?] for discussions on the applicability of this method.

4.1 Global SNO signal and other neutrino oscillation data

For the purpose of this analysis, the χ^2 can be considered as the sum of three distinct contributions:

$$\chi^2 = \chi_{\text{KL}}^2 + \chi_{\odot/\text{SNO}}^2 + \chi_{\text{glob,SNO}}^2 \quad (8)$$

where χ_{KL}^2 is as in Eq. 7.

We define $\chi_{\odot/\text{SNO}}^2$ as the contribution of all solar neutrino experiments except SNO, i.e. (see Eq. 4, 7):

$$\chi_{\odot/\text{SNO}}^2 = \chi_{\text{rad}}^2 + \chi_{\text{SK}}^2 \quad (9)$$

The SNO contribution is given by

$$\chi_{\text{glob,SNO}}^2 = (\mathbf{R}^{\text{th}} - \mathbf{R}^{\text{exp}})^T (\sigma_{\text{corr}} + \sigma_{\text{syst}})^{-1} (\mathbf{R}^{\text{th}} - \mathbf{R}^{\text{exp}}) \quad (10)$$

where $\mathbf{R}^{\text{th,exp}}$ are length-14 vectors containing the phase-II spectrum data (13 bins) and the new phase-III global SNO result. We consider the two SNO results as if coming from two independent experiments, but fully correlated. We use the backgrounds as listed in table 1 of [6] for the phase-II data, and the detector resolution given in the HOWTO.

4.2 The SNO spectrum and other neutrino oscillation data

As mentioned previously, the SNO collaboration does not analyze the full spectrum data. We prefer to take it into consideration in order to be able to make the comparison between our new analysis and previous work on the SNO results more easy. We therefore consider the full SNO phase-II and phase-III data (listed in Table 1). The $\chi_{\text{spect,SNO}}^2$ has the same formal expression as Eq. 10, where it is understood that $\mathbf{R}^{\text{th,exp}}$ are now length 26 vectors containing two 13-bin relative to the two SNO data sets. We consider the two fully correlated.

The difficulty in using the spectrum data lies in correctly estimating the systematics. By using the information contained in Table II of [3], we have computed the influence of all the different sources of error on our response function considering the correlation/anti-correlation as presented in Table 1 of [9]. The different backgrounds present yet another difficulty, because we have access only to the total number of background events coming from the different sources listed in Table I of [3]. We have taken the background spectrum presented in the phase-II paper and normalized it to the total number of events in the $\text{D}_2\text{O} + \text{NaCl}$ phase.

Table 1: Energy spectrum observed at SNO (taken from fig. 2 of ref [3]).[†]

T_{eff} (MeV)	Events per 500 keV	T_{eff} (MeV)	Events per 500 keV
5.5- 6.0	510	9.0- 9.5	130
6.0- 6.5	515	9.5-10.0	120
6.5- 7.0	475	10.0-10.5	60
7.0- 7.5	385	10.5-11.0	70
7.5- 8.0	300	11.0-11.5	40
8.0- 8.5	240	11.5-12.0	35
8.5- 9.0	145		

[†] It contains the CC, ES, and NC + internal and external source neutron events.

5 Our results

In table 6 we report the values of the mixing parameters Δm_{\odot}^2 , $\tan^2 \theta_{\odot}$, and the χ^2 obtained from minimization and from the peak of marginal likelihood distribution.

In fig. 6-(left) we show the exclusion plots for the solar and kamLAND spectrum, with the global signal of the SNO phase-III data, whereas the right pannel refers to the kamLAND spectrum, radiochemical + cherenkov solar data and the SNO phase-III spectrum information. Contour lines correspond to the the allowed areas at 90, 95, 99 and 99.7% CL relative to the absolute minimum.

In fig. 6 we plot the marginalized likelihood distributions for each of the oscillation parameters Δm^2 , and $\tan^2 \theta$ corresponding to the Kamland Spectrum plus solar evidence. The values for the peak positions and their widths are obtained by fitting two-sided Gaussian distributions and are given in Table 6.a.

6 Summary and Conclusions

We have presented an up-to-date analysis of all solar neutrino experimental data, including the SNO phase-III spectrum and recent KamLAND results. The (predominantly) active neutrino oscillations hypothesis has been confirmed, and the decoupling of the atmospheric Δm^2 -solar Δm^2 justifies a 2-flavour analysis.

The inclusion of the new KamLAND data determines at good accuracy the value of Δm_{\odot}^2 and brings us to a new era of precision measurements in the solar neutrino parameter space [22]. Furthermore, the slight asymmetry present in the kamLAND data alone around the $\tan^2 \theta = 1$ indicates that $\Delta m_{21}^2 > 0$. Improvement on the determination of $\tan^2 \theta$ is still needed and will only be possible with new data from solar neutrino experiments, eg Superkamiokande. The use of the SNO phase-III spectrum in the data set has a slight effect in reducing the overall area of allowed parameters, but leaves the best-fit $\tan^2 \theta$ inalterred, only slightly changing the best-fit Δm_{\odot}^2 .

The (lower) accuracy with which we determine the solar mixing angle is evident in the marginalized likelihood plots of fig. 6. Our best-fit points are.

References

- [1] T. Araki *et al.* [KamLAND Collaboration], ArXiv:hep-ex/0406035.
- [2] A. B. Balantekin, V. Barger, D. Marfatia, S. Pakvasa and H. Yuksel, arXiv:hep-ph/0405019.
L. Oberauer, Mod. Phys. Lett. A **19** (2004) 337 [arXiv:hep-ph/0402162].

- [3] S. N. Ahmed *et al.* [SNO Collaboration], Phys. Rev. Lett. **92** (2004) 181301 [arXiv:nucl-ex/0309004].
- [4] J. Boger *et al.* [SNO Collaboration], Nucl. Instrum. Meth. A **449**, 172 (2000)
- [5] A. W. Poon [SNO Collaboration], arXiv:nucl-ex/0110005.
- [6] Q. R. Ahmad *et al.* [SNO Collaboration], Phys. Rev. Lett. **89** (2002) 011301, Q. R. Ahmad *et al.* [SNO Collaboration], Phys. Rev. Lett. **89** (2002) 011302.
- [7] G.L. Fogli, E. Lisi, A. Palazzo, A.M. Rotunno, Phys. Rev. D **67**, 073001 (2003)
- [8] G. L. Fogli, E. Lisi, A. Marrone and A. Palazzo, Phys. Lett. B **583** (2004) 149 [arXiv:hep-ph/0309100].
- [9] “HOWTO use the SNO Salt Flux Results,” [SNO Collaboration], can be found at <http://www.sno.phy.queensu.ca>
- [10] K. Eguchi *et al.* [KamLAND Collaboration], Phys. Rev. Lett. **90**, 021802 (2003).
- [11] A. B. Balantekin and H. Yuksel, J. Phys. G **29**, 665 (2003), P. Aliani, V. Antonelli, M. Picariello and E. Torrente-Lujan, Phys. Rev. D **69** (2004) 013005 [arXiv:hep-ph/0212212]. H. Nunokawa, W. J. Teves and R. Zukanovich Funchal, Phys. Lett. B **562**, 28 (2003) J. N. Bahcall, M. C. Gonzalez-Garcia and C. Pena-Garay, JHEP **0302**, 009 (2003) A. Bandyopadhyay, S. Choubey, R. Gandhi, S. Goswami and D. P. Roy, Phys. Lett. B **559**, 121 (2003) M. Maltoni, T. Schwetz and J. W. Valle, Phys. Rev. D **67**, 093003 (2003) G. L. Fogli, E. Lisi, A. Marrone, D. Montanino, A. Palazzo and A. M. Rotunno, Phys. Rev. D **67**, 073002 (2003) V. Barger and D. Marfatia, Phys. Lett. B **555**, 144 (2003) P. C. de Holanda and A. Y. Smirnov, JCAP **0302**, 001 (2003) A. B. Balantekin and H. Yuksel, J. Phys. G **29**, 665 (2003).
- [12] R. Davis, Prog. Part. Nucl. Phys. 32 (1994) 13. B.T. Cleveland et al., (HOMESTAKE Coll.) Nucl. Phys. (Proc. Suppl.) **B 38** (1995) 47. B.T. Cleveland et al., (HOMESTAKE Coll.) Astrophys. J. 496 (1998) 505-526.
- [13] J.N. Abdurashitov et al. (SAGE Coll.) Phys. Rev. Lett. 83(23) (1999)4686.
- [14] A.I. Abazov et al. (SAGE Coll.), Phys. Rev. Lett. **67** (1991) 3332. D.N. Abdurashitov et al. (SAGE Coll.), Phys. Rev. Lett. **77** (1996) 4708. J.N. Abdurashitov et al., (SAGE Coll.), Phys. Rev. **C60** (1999) 055801; astro-ph/9907131. J.N. Abdurashitov et al., (SAGE Coll.), Phys. Rev. Lett. **83** (1999) 4686; astro-ph/9907113.
- [15] P. Anselmann et al., GALLEX Coll., Phys. Lett. **B 285** (1992) 376. W. Hampel et al., GALLEX Coll., Phys. Lett. **B 388** (1996) 384. T.A. Kirsten, Prog. Part. Nucl. Phys. 40 (1998) 85-99. W. Hampel et al., (GALLEX Coll.) Phys. Lett. **B 447** (1999) 127. M. Cribier, Nucl. Phys. (Proc. Suppl.) **B 70** (1999) 284. W. Hampel et al., (GALLEX Coll.) Phys. Lett. **B 436** (1998) 158. W. Hampel et al., (GALLEX Coll.) Phys. Lett. **B 447** (1999) 127.
- [16] M. Altmann et al. (GNO Coll.) Phys. Lett. B490 (2000) 16-26.
- [17] J. N. Bahcall, M. H. Pinsonneault and S. Basu, Astrophys. J. **555**, 990 (2001).
- [18] P. Aliani, V. Antonelli, M. Picariello and E. Torrente-Lujan, arXiv:hep-ph/0212212. P. Aliani, V. Antonelli, M. Picariello and E. Torrente-Lujan, New J. Phys. **5**, 2 (2003). P. Aliani, V. Antonelli, R. Ferrari, M. Picariello and E. Torrente-Lujan, Phys. Rev. D **67**, 013006 (2003). P. Aliani, V. Antonelli, M. Picariello and E. Torrente-Lujan, Nucl. Phys. B **634**, 393 (2002).
- [19] M. B. Smy, arXiv:hep-ex/0202020.
- [20] M. Apollonio et al. (CHOOZ coll.) Phys. Lett. **B 466** (1999) 415; M. Apollonio *et al.*, Phys. Lett. **B 420** (1998) 397.
- [21] Y. F. Wang [Palo Verde Collaboration], Int. J. Mod. Phys. A **16S1B**, 739 (2001); F. Boehm *et al.*, Phys. Rev. D **64**, 112001 (2001).
- [22] see <http://neutrino2004.in2p3.fr> for KamLAND transparencies and Global analysis (S. Goswami)

Experiment	Data	References
Homestake		[12]
SAGE		[13, 14]
GallEx		[15]
GNO		[16]
SuperKamiokande		[19]
SNO		[3]
CHOOZ		[20]
Palo Verde		[21]
KamLAND		[1, 10]

Table 2: Data and references used in our analysis

	$\Delta m^2(\text{eV}^2)$	$\tan^2 \theta$
from χ^2 minimization		
KL (Sp+Gl)+Solar + SNO (Sp)	7.89×10^{-5}	0.40
KL (Sp+Gl)+Solar + SNO (Gl)	8.17×10^{-5}	0.40
from marginalization		
KL (Sp+Gl)+Solar + SNO (Sp)	$8.2_{-0.8}^{+0.9} \times 10^{-5}$	$0.50_{-0.6}^{+0.12}$

Table 3: Mixing parameters from χ^2 minimization and likelihood marginalization.

Bin (MeV)	S_{exp}/MC	$\sigma_{\text{stat.}} (\%)$
2.600 - 3.025	0.45	1.4
3.025 - 3.450	0.56	1.5
3.450 - 3.875	0.67	1.7
3.875 - 4.300	0.62	2.1
4.300 - 4.725	0.99	2.6
4.725 - 5.150	1.20	3.3
5.150 - 5.575	0.80	4.5
5.575 - 6.000	1.00	6.7
6.000 - 6.425	1.20	10.0
6.425 - 6.850	0.33	17.0
6.850 - 7.275	0.67	33.0
7.275 - 7.700	0.00	-
7.700 - 8.125	-	-

Table 4: Summary of Kamland spectrum information extracted from [1]. Relative statystical errors only are reported.

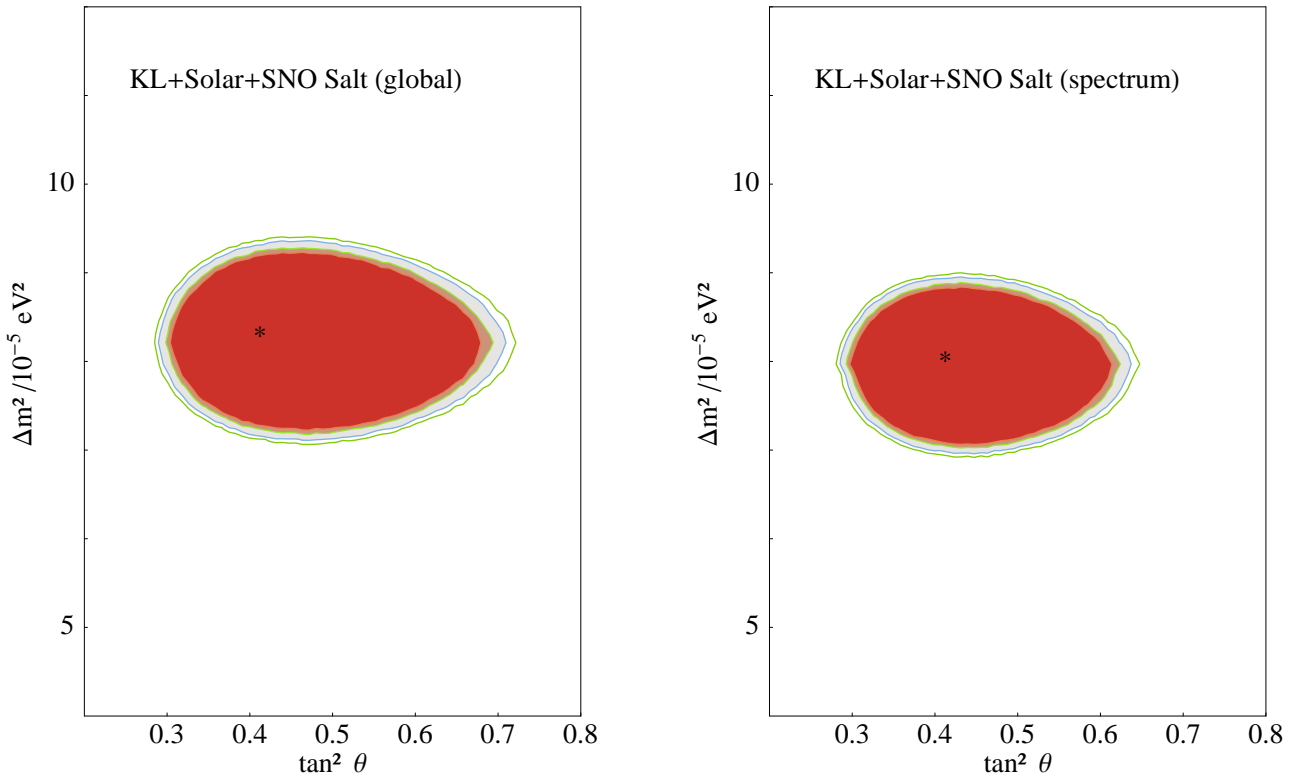


Figure 1: (left) Allowed region in the $(\tan^2 \theta, \Delta m^2_\odot)$ plane for the global analysis, which includes the previous solar data (see e.g. [18] for details) and all kamLAND Global results. (right) Best fit solution for the spectrum analysis, including all previous solar data, short baseline reactor data and the kamLAND spectrum. Best fit point given in table 3.

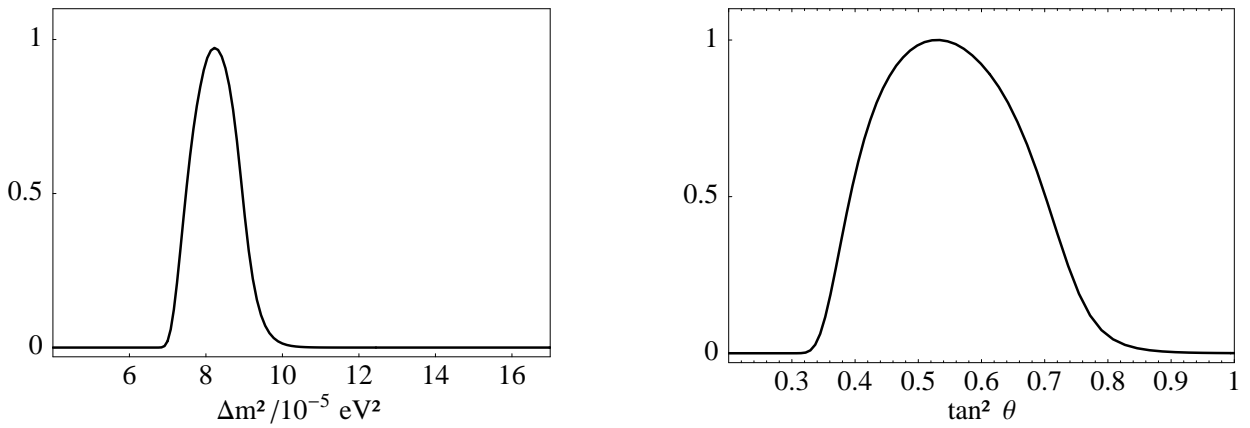


Figure 2: marginalized likelihood distributions for each of the oscillation parameters Δm_\odot^2 (left) and $\tan^2 \theta$ (right) corresponding to the totality of solar and KamLAND data. The curves are in arbitrary units with normalization to the maximum height.